Title

Conversion reaction of vanadium sulfide electrode in the lithium-ion cell: Reversible or not reversible?

Authors

Zhang, Liang
Wei, Qiulong
Sun, Dan
et al.

Publication Date

2018-09-01

DOI

10.1016/j.nanoen.2018.06.076

Peer reviewed

Understanding the Electrochemical Reaction Mechanism of VS_2 Nanosheets in Lithium-Ion cells by Multimodal in situ and ex situ X-ray Spectroscopies

Liang Zhang,[1] Dan Sun,[2] Qiulong Wei,[3] Huanxin Ju,[4] Jun Feng,[1] Junfa Zhu,[4] Liqiang Mai,[3]

Elton J. Cairns,[2,5] Jinghua Guo[1,6*]

1. Advanced Light Source, Lawrence Berkeley National Laboratory, Berkeley, California 94720, United States
2. Energy Storage and Distributed Resources Division, Lawrence Berkeley National Laboratory, Berkeley, California 94720, United States
3. State Key Laboratory of Advanced Technology for Materials Synthesis and Processing, International School of Materials Science and Engineering, Wuhan University of Technology, Wuhan 430070, China
4. National Synchrotron Radiation Laboratory, University of Science and Technology of China, Hefei 230029, China
5. Department of Chemical and Biomolecular Engineering, University of California, Berkeley, California 94720, United States
6. Department of Chemistry and Biochemistry, University of California, Santa Cruz, California 95064, United States

*Email: jguo@lbl.gov

Abstract

Recently two-dimensional layered transition metal dichalcogenides (TMDs) have attracted great scientific interest in electrochemical energy storage. As an important family member of TMDs, vanadium disulfide (VS_2) is a promising electrode material for lithium-ion cells because of its remarkable electrical conductivity and fast Li^+ diffusion rate, but its electrochemical reaction mechanism is still poorly understood. Herein, we have prepared an electrode consisting of VS_2 nanosheets and systematically investigated its structural and chemical evolution during the electrochemical processes by employing both *in situ* and *ex situ* X-ray spectroscopies. The VS_2 undergoes intercalation and conversion reactions in sequence during discharge and this process is found to be partially reversible during the subsequent charge. The decreased reversibility of the conversion reaction over extended cycles could be mainly responsible for the capacity fading of the VS_2 electrode. In addition, the hybridization strength between S and V shows a strong dependence on the states of charge, as directly proved by the intensity change of the V-S hybridized states and pure V states. We also reveal that the solid electrolyte interphase on the electrode surface is dynamically evolved during cycling, which may be a universal phenomenon for conversion-based electrodes. This study is expected to be beneficial for the further development of high-performance VS_2-based electrodes.

Keywords: VS_2 nanosheets, lithium ion batteries, electronic structure, solid electrolyte interphase, X-ray absorption spectroscopy, resonant inelastic X-ray scattering

Lithium-ion batteries (LIBs) have been extensively developed as the leading energy storage devices in portable electronics and electric vehicles.[1-6] However, the relatively low theoretical capacities of the commercial electrodes (e.g., 372 mAh/g for graphite and 170 mAh/g for $LiCoO_2$) are insufficient for the ever-increasing demands of society.[7] As a consequence, enormous efforts have been devoted to the exploration of new electrode materials with lower costs and higher energy densities.

Transition metal dichalcogenides (TMDs) have attracted intensive attention in electrochemical energy storage recently owing to their unique layered structures and versatile electronic and chemical properties.[8-9] For example, MoS_2 has been largely explored as the anode material for LIBs due to its high theoretical capacity and fast lithium ion diffusion rate.[10-12] However, the intrinsically low electrical conductivity of MoS_2 seriously inhibits its electrochemical performance, especially under high current conditions. In contrast, VS_2, another important member of TMDs, demonstrates an intrinsic metallic behavior and a faster lithium ion diffusion rate than that of MoS_2 and graphite,[13-15] which makes VS_2 a promising electrode material for LIBs. For instance, Fang *et al.* showed that a hierarchical VS_2/graphene nanosheet electrode exhibited a high reversible capacity of 528 mAh/g at a specific current of 0.2 A/g after 100 cycles.[16] More recently, Zhou *et al.* synthesized ultrathin VS_2 nanosheets with a few atomic layer thickness, which delivered a remarkably high capacity up to 1000 mAh/g at a current density of 0.1 A/g and 570 mAh/g at a specific current of 10 A/g.[17] These reports were mainly focused on the improvement of the electrochemical performance of VS_2-based electrode materials, whereas little attention has been paid to the detailed mechanism of the redox process and the reason for the capacity fading, which can be beneficial for the better modification of the VS_2 structure to achieve a superior electrochemical performance.[17-20]

In this work, we synthesized layer-by-layer stacked VS_2 nanosheets using a facile polyvinylpyrrolidone (PVP) assisted method. We then applied multimodal *in situ* and *ex situ* X-ray spectroscopies, including hard (V K-edge), tender (S K-edge), and soft (V L-edge, C and O K-edge) X-ray absorption spectroscopy (XAS) as well as resonant inelastic X-ray scattering (RIXS, V L-edge), to investigate the evolution of the structural, physical, and chemical properties of the VS_2 nanosheets used as the electrode material for LIBs in order to understand the electrochemical reaction and capacity fading mechanism. The advantage of XAS and RIXS is that they are element-resolved and highly sensitive to the local chemical bonding

environments, and provide a deep insight into the electronic structures of both occupied and unoccupied partial density of states (PDOS) of the investigated materials.[21-22] The qualitative and quantitative analysis of the *in situ* and *ex situ* X-ray spectroscopies provides valuable information about the redox process and the formation process of the solid electrolyte interphase (SEI) layer for the VS_2 nanosheet electrodes.

Experimental details

Synthesis of VS_2 nanosheets

1 g PVP K-30 was first dissolved in the mixture of ammonium hydroxide (2 ml) and distilled water (30 ml) and then 2 mmol NH_4VO_3 was dissolved with continuous stirring following the addition of 20 mmol C_2H_5NS (TAA). The solution was loaded into an autoclave and maintained at 180 °C for 20 h. After that, the obtained suspension was centrifuged and washed with distilled water and ethanol and then dried at 60°C for 12 h in a vacuum oven. Last, the products were annealed at 300°C for 2 h to obtain VS_2 nanosheets.

Cell preparation and electrochemical cycling

The VS_2 electrodes were prepared by mixing active materials, super P, and PVDF binder at a weight ratio of 7:2:1. The slurries were then coated onto a commercial copper foil. CR2325 coin cells were assembled in an argon-filled glove box using lithium foil as the counter electrode and 1 M LiPF6 in EC/DEC (1:1, by volume) as the electrolyte. The electrochemical performance of the cells was evaluated between 0.05 V and 3.0 V using a battery cycler (Arbin BT2000). The cyclic voltammograms were measured using a Biologic electrochemical workstation at a scan rate of 0.1 mV/s.

In situ and ex situ X-ray absorption spectroscopy measurements

The *in situ/operando* and *ex situ* S and V K-edge XAS spectra were measured at beamline 5.3.1 at the Advanced Light Source (ALS), Lawrence Berkeley National Laboratory (LBNL). The *in situ* electrochemical cells were adapted from the CR2325 coin cells, as described in our previous reports.[23-24] The ex situ V L-edge, C and O K-edge XAS spectra and V L-edge RIXS maps were measured at beamline 8.0.1 at the ALS, LBNL. The photoemission spectroscopy experiments were performed at the Catalysis and

Surface Science Endstation at the BL11U beamline in the National Synchrotron Radiation Laboratory (NSRL) in Hefei, China.

Results and discussion

The phase of as prepared VS_2 nanosheets was identified by X-ray diffraction (XRD), as shown in Figure 1a. All the XRD peaks correspond to the typical diffraction peaks of hexagonal VS_2 with a space group of *P*-3*m*1 (PDF No. 036-0019), indicating the successful formation of VS_2 without any side reaction. The Raman spectrum (Figure 1b) shows three peaks located at 282, 300, 405 cm^{-1}, which are assigned to the E_{1g}, E^1_{2g}, and A_{1g} vibrational bands of VS_2, respectively.[17-18] The V 2p X-ray photoemission spectroscopy (XPS) spectrum shows two peaks at 517.01 and 524.36 eV, corresponding to the V $2p_{3/2}$ and V $2p_{1/2}$ states due to the spin-orbital splitting effect, respectively. In addition, the V 2p peak positions are very similar to those of VO_2,[25] indicating that the V atoms in VS_2 are mainly present as V^{4+}. To investigate the morphology of the as synthesized VS_2, we further performed scanning electron microscopy (SEM). The SEM image (Figure 1d) reveals that VS_2 is composed of layer-by-layer stacked nanosheets with a lateral size of several μm. The thickness of the VS_2 nanosheets is estimated to be ~20 nm. Moreover, the energy dispersive spectrometry (EDS) results exhibit a similar distribution of V and S in the VS_2 nanosheets (Figure 1e-f). This unique layer-by-layer structure of VS_2 could be beneficial for the rapid and durable lithium ion storage.

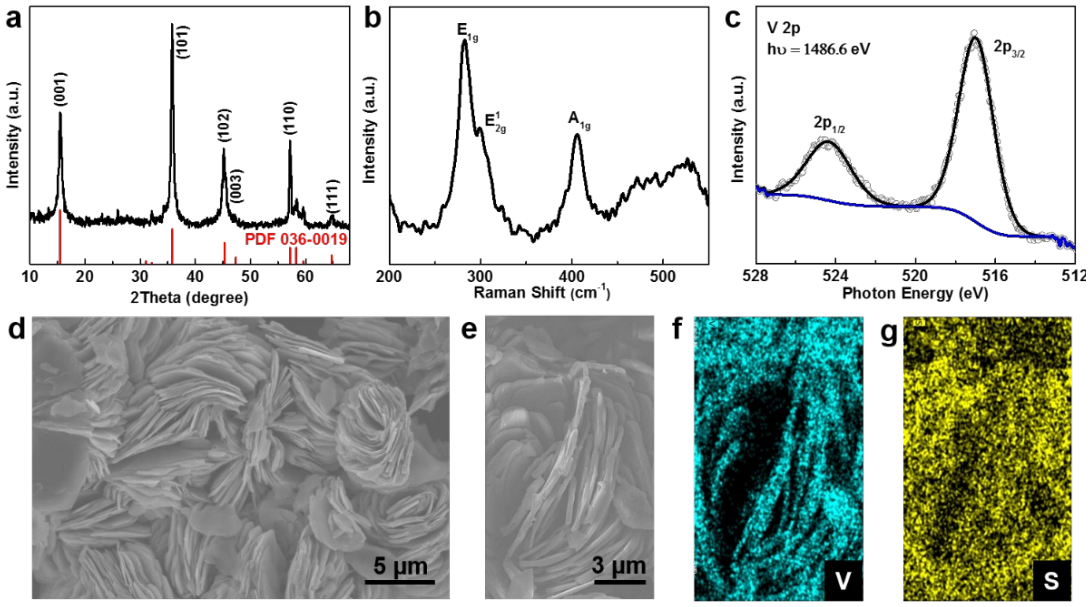

Figure 1. Structure characterization of synthesized VS_2 nanosheets. (a) XRD pattern. (b) Raman spectrum. (c) V 2p XPS spectrum. (d) SEM image. (e-g) EDS elemental mapping of V and S.

To evaluate the electrochemical performance of the VS_2 nanosheets for LIBs, we paired the active materials with metallic lithium foils in standard coin cells and then cycled them in the voltage range of 0.05-3.0 V at a specific current of 0.2 A/g. Figure 2a shows the discharge-charge voltage profiles of the initial two cycles. Two plateaus near 1.4 and 0.8 V are observed in the first discharge curve, which correspond to the intercalation $\begin{matrix} -¿ \rightarrow Li_xVS_2 \\ +¿+x\,e^{¿} \\ VS_2+xLi^{¿} \\ ¿ \end{matrix}$ and conversion $\begin{matrix} -¿ \rightarrow 2Li_2S+V \\ +¿+(4-x)\,e^{¿} \\ Li_xVS_2+(4-x)\,Li^{¿} \\ ¿ \end{matrix}$ reactions, respectively.[17] It has been predicted that the theoretical specific capacity of VS_2 for lithium intercalation can reach up to 466 mAh/g, which corresponds to the formation of Li_2VS_2 (i.e., $0 \le x \le 2$ ¿ .[13,15,26] In contrast, a series of plateaus are observed in the charge voltage profile. The first discharge and charge capacities are 1580 and 1138 mAh/g, respectively. The relatively low Coulombic efficiency (72%) could be related to the decomposition of electrolyte and formation of a SEI layer. The corresponding plateaus are still discernable in the second cycle, suggesting that the lithium intercalation and conversion reactions are reversible.

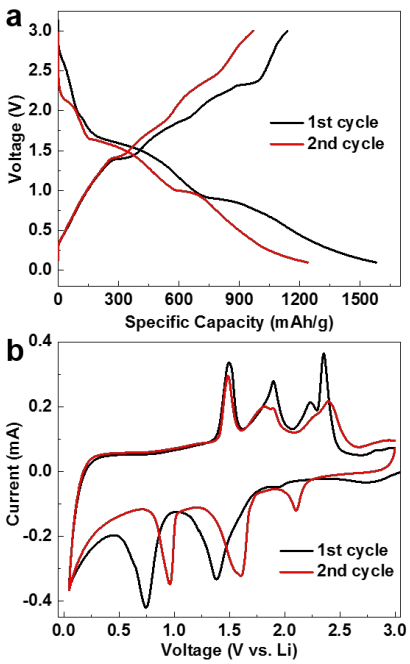

Figure 2. Electrochemical characterization of VS_2 nanosheets. (a) Discharge/charge voltage profiles at a scan rate of 0.2 A/g. (b) Cyclic voltammograms at a scan rate of 0.1 mV/s.

In order to better understand the lithium intercalation and conversion reaction mechanisms, we further performed cyclic voltammetry (CV) for VS_2 in the voltage range of 0.05-3.0 V at a scan rate of 0.1 mV/s, as depicted in Figure 2b. Consistent with the discharge voltage profile, two reduction peaks centered at 1.4 and 0.75 V corresponding to the intercalation reaction and conversion reactions are observed in the first cathodic scan. The reduction peaks shift to higher potentials in the subsequent cathodic scan. This observation is probably due to the partial irreversible structure change after the first cycle.[24] Several oxidation peaks are observed in the anodic scans, suggesting a multistep delithiation process of VS_2. Note that a new reduction peak appears at 2.1 V in the second cathodic scan, which may be related to the phase change of VS_2 during lithium intercalation or the adsorption of lithium at the defect sites of VS_2.[16] The exact origin of this peak is not yet fully understood at the moment and further investigation is highly recommended.

To further understand the electrochemical reaction mechanism of VS_2 electrodes, we performed an *in situ* and operando S and V K-edge XAS experiment to evaluate the local structural and chemical evolution of

VS_2 during the discharge and charge processes. Figure 3a-e and 3f-g show the voltage profiles, the *in situ* and operando S and V K-edge XAS maps, and the representive XAS spectra of VS_2 during the first discharge and charge processes in real time, respectively. Note that the voltage was held at the cutoff voltage for 1.5 h at the end of discharge and charge to ensure a full reaction of VS_2 (Figure 3a and f). For S K-edge XAS spectra (Figure 3b, c, g, h), the main features located at 2470.3 and 2471.6 eV are attributed to the t_{2g} and e_g states induced by the hybridization between S 3p and V 3d states, while the broad feature at 2480 eV reflects the S 3p-V 4s, p hybridized states. As shown in Figure 3b and c, the intensity of t_{2g} and e_g states decreased continuously during lithium intercalation process. In addition, it seems that the t_{2g} state is more influenced by lithium intercalation than the e_g state. These observations indicate that the electrons are also partially transferred to the t_{2g} states of sulfur during discharge, resulting in the decreased transition probability of sulfur 1s to these levels during the X-ray absorption process. This means that the sulfur is also electrochemically active and participated in the redox process. The involvement of anionic redox for the VS_2 electrode is most likely due to the overlap between S 3p states and V 3d states.[15] A similar phenomenon has also been observed for TiS_2 during the discharge and charge processes.[27] With further discharge, the t_{2g} and e_g states totally disappear, and instead, two broad features at 2473.5 and 2476.6 eV are developed. The spectrum collected at the end of discharge is very similar to that of Li_2S,[24,28] indicating the conversion from VS_2 to Li_2S. Upon recharging the electrode to 3.0 V (Figure 3g and h), the characteristic t_{2g} and e_g states of VS_2 are gradually recovered, indicative of the reversible intercalation and conversion reactions of VS_2 in the first cycle.

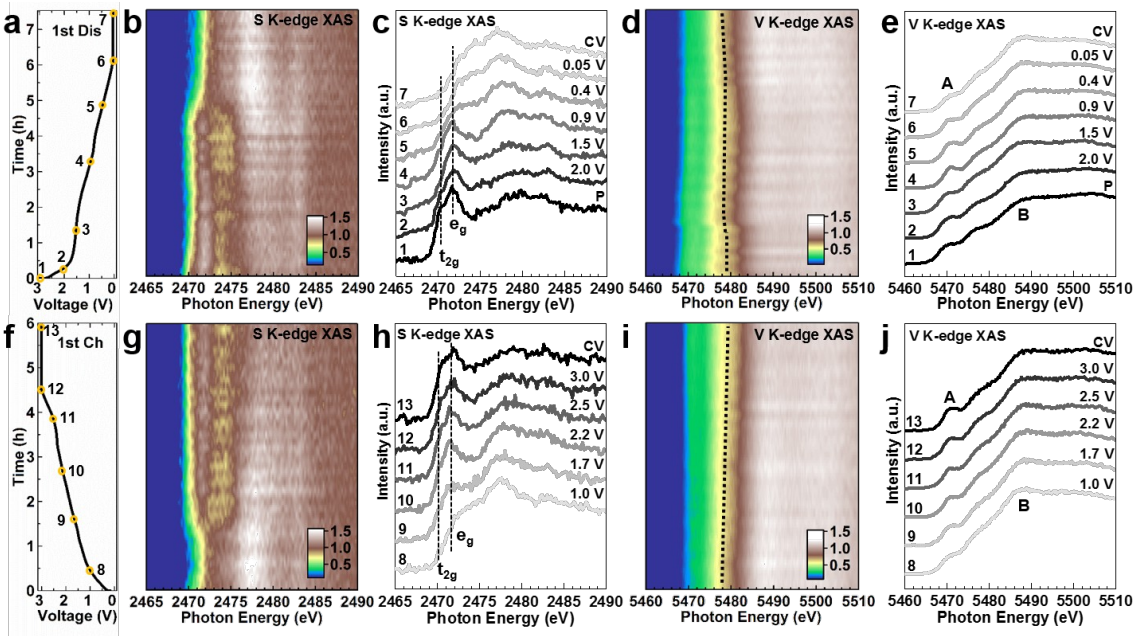

Figure 3. *In situ* and operando S and V K-edge XAS of VS_2 electrodes for the first cycle. (a) Discharge voltage profile at a specific current of 0.2 A/g for the *in situ* and operando XAS measurement. (b) Operando S K-edge XAS map and (c) representive XAS spectra during the first discharge process. (d) Operando V K-edge XAS map and (e) representive XAS spectra during the first discharge process. (f) Charge voltage profile at a specific current of 0.2 A/g for the in situ and operando XAS measurement. (g) Operando V K-edge XAS map and (h) representive XAS spectra during the first discharge process. (i) Operando V K-edge XAS map and (j) representive XAS spectra during the first discharge process.

The *in situ* and operando V K-edge XAS results further confirm the reversibility of the electrochemical reaction of VS_2 (Figure 3d, e, i, and j). For the spectrum of pristine VS_2, the distinctive pre-edge peak A at ~5470 eV is attributed to the dipole-forbidden V 1s to 3d transition.[29] The presence of this peak implies a slightly distorted octahedral symmetry of V atoms in VS_2, and the intensity of this peak is strongly dependent on the local coordination environment of V atoms.[29-30] The main absorption peak B at ~5490 eV corresponds to the V 1s to 4p transition. During the discharge process, a shift of the main absorption edge to lower energies is clearly observed, reflecting the reduction of the oxidation state of V.[31-32] In addition, the intensity of the pre-edge peak also gradually decreases, which is induced by the symmetry change of V atoms as a result of lithiation. Actually, the lithiation induced local coordination environment change of metal atoms has also been observed for other conversion electrodes, e.g., $NiFe_2O_4$,[33] TiS_4,[34] and FeS_2.[35] Note

that the spectrum at the end of discharge is still different from that of V metal, which may be related to the small domain size of the as formed metal clusters and/or the interaction between formed Li_2S and V metal.[36-38] During the subsequent charge to 3.0 V, the intensity of the pre-edge peak increases and the main absorption edge shifts back to higher energies, indicating the recovery of the symmetry and the gradual oxidation of V atoms. Overall, the *in situ* and operando S and V K-edge XAS results clearly demonstrate that the electrochemical reaction of VS_2 is reversible in the first cycle and both S and V are involved in the redox reactions during the electrochemical processes.

In order to confirm the changes observed in the *in situ* and operando results, we also measured the *ex situ* S and V K-edge XAS for the VS_2 electrodes at different states of charge (Figures S1 and S2). The results show similar changes to those observed in the *in situ* and operando results, confirming the relatively high reversibility of the intercalation and conversion reactions of VS_2 during the first cycle. However, a gradual decrease of the reversibility of the reactions is observed after 2 and 10 cycles (Figures S1 and S2), which could be a main reason for the capacity fading of the VS_2 electrode.

Although the above V K-edge XAS results clearly reveal the structural and chemical change of VS_2 during the cycling process, it would be more convincing if we can directly probe the evolution of the V 3d states.[39] We therefore further performed *ex situ* V L-edge XAS and RIXS on a series of VS_2 electrodes at different states of charge and discharge (Figure 4a) to understand the evolution of unoccupied and occupied V 3d states. Figures 4b and c show the V L-edge XAS spectra of the VS_2 electrodes cycled to different voltages in both total electron yield (TEY, ~5nm detection depth) and total fluorescence yield (TFY, ~100 nm detection depth) modes, respectively.

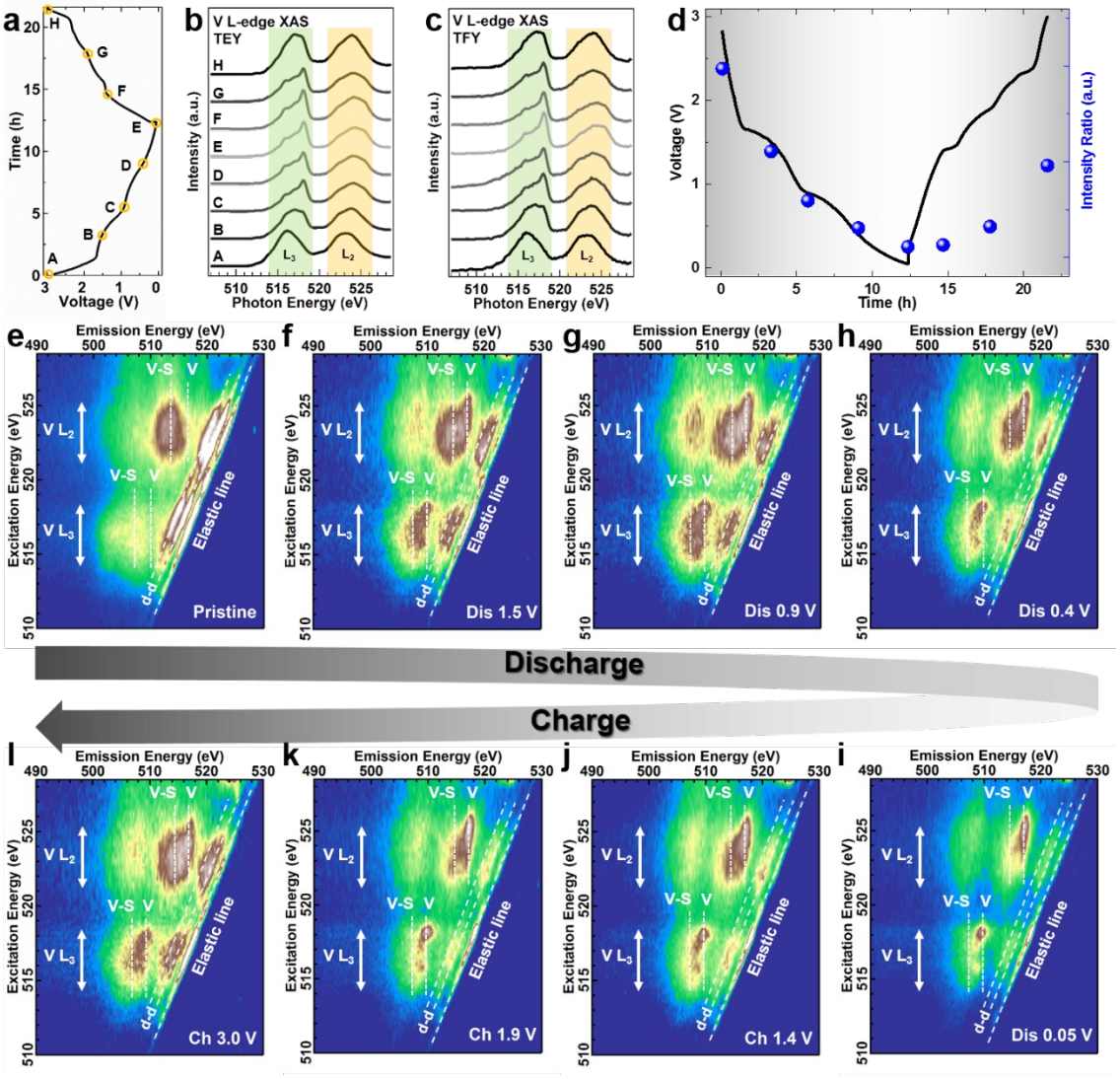

Figure 4. Ex situ V L-edge XAS spectra and RIXS maps of VS_2 electrodes at different states of charge in the first cycle. The samples are pristine (A), 1.5 V discharge (B), 0.9 V discharge (C), 0.4 V discharge (D), 0.05 V discharge (E), 1.4 V charge (F), 1.9 V charge (G), and 3.0 V charge (H), as indicated in the corresponding voltage profile (a). The spectra were measured through the current collector side. (b) and (c) V L-edge XAS spectra collected in TEY and TFY modes, respectively. (d) Intensity ratio evolution of the V 3d-S 3p hybridized states to the pure V 3d states as a function of discharge and charge voltages. (e-i) V L-edge RIXS maps of VS_2 at different states of charge throughout the first cycle.

The two main regions of the XAS spectra can be assigned to the L_3-edge ($2p_{3/2}$ to 3d) at 514-519 eV and L_2-edge ($2p_{1/2}$ to 3d) at 521-526 eV, originated from the spin-orbital splitting.[29] We mainly focus on the line

shape evolution of the L_3-edge because the L_2-edge demonstrates broader features owing to the shorter lifetime of the $2p_{1/2}$ states and the Coster-Kronig Auger decay process.[22] It is clear that the shape of the L_3-edge shows a strong dependence on the state of charge. More specifically, the intensity of the feature located at ~516 eV continuously decrease during discharge (spectra A-E) and increases during charge (spectra E-H). Note that the evolutions of the spectra collected in TEY and TFY modes are similar, indicating that the oxidation state changes of V are similar for the surface and bulk of VS_2 electrodes at the current collector side. The evolution of the absorption spectra can be interpreted by the redox reaction of V in VS_2. The occupancy of V 3d states is increased (decreased) during discharge (charge), resulting in the change of the oxidation state of V. The modification of the oxidation state of V and the resultant change of metal-ligand bonding strength thus lead to a distinct change of the XAS signatures. It is very likely that the electrons are mainly transferred to the low-energy d orbitals (d_{xy}, d_{xz}, and d_{yz}) upon discharge, and therefore the spectral shape change mainly occurs at the low energy region of the L_3-edge.[40-41] At the end of charge back to 3.0 V, the V L-edge line shape (spectrum H) is not fully recovered to that of pristine VS_2. These observations, consistent with the V K-edge XAS results, indicate that the redox reaction of V is only partially reversible during the first cycle, which explains the low Coulombic efficiency observed in the electrochemical results. Moreover, the V L-edge XAS also demonstrates a gradually decreased reversibility of the conversion reaction of VS_2 (Figure S3), in good agreement with the V K-edge XAS results.

The occupied electronic structure change of V 3d states during the cycling process is further investigated by V L-edge RIXS. The RIXS results map the fluorescence intensity as a function of excitation (ordinate) and emission (abscissa) energies. For the pristine electrode, the RIXS map consists of energy-loss features (d-d orbital excitations) that are parallel to the elastic line and normal fluorescence features that have fixed emission energies (vertical stripes in the map). The occurrence of the strong d-d excitations is an indication of the heavily correlated nature of the electronic structure of VS_2.[42] The emission features located at 504-512 eV and 512-520 eV are assigned to the V L_α and V L_β bands, respectively.[29,42-43] The intensity of the d-d excitations gradually decreases during discharging to 0.05 V, and then increases after charging back to 3.0 V. As the d-d excitations are highly sensitive to hybridization strength of the metal d states and ligand p states (the higher the strength, the stronger the d-d excitations),[44-45] the evolution of the d-d excitations

observed in the RIXS maps provides direct evidence that the hybridization strength between V 3d states and S 3p states is depressed during discharge and enhanced during charge.

This scenario is further verified by the change of the fluorescence features of V L_α and V L_β bands. The emission features at 514.5 eV (507.0 eV) and 517 eV (509.5 eV) of the V L_β (L_α) band originate from the V 3d states strongly hybridized with S 3p states (marked as V-S in the RIXS maps) and the pure V 3d states (marked as V in the RIXS maps), respectively, according to the calculated density of states of VS_2.[13,15] The weight of hybridized states is dominant for pristine VS_2. In contrast, the weight of pure V states becomes dominant with increasing lithiation, while it is greatly decreased during the subsequent delithiation. To quantitatively understand the evolution of these states, we have plotted the intensity ratio of the hybridized states and pure V states as a function of state of charge, as shown in Figure 4d. The intensity values were derived from the RIXS spectra excited at the L_2 edge maximum of the corresponding XAS spectra (Figure S4). The intensity ratio evolution clearly reflects the transformation of the hybridized states to the pure V states during discharge due to the conversion from VS_2 to metallic V, which is consistent with the change of d-d excitations. However, the intensity ratio is not fully recovered to the pristine one at the end of charge, implying that the lithium is not fully extracted, consistent with the V L-edge XAS results. A similar intensity ratio evolution is also observed after 2 and 10 cycles (Figure S4 and S5). However, the intensity ratio change weakenes progressively, indicating a gradual decrease of the reversibility of the lithium intercalation and conversion reactions of VS_2. Again, this could be the main reason for the capacity degradation of VS_2 electrode with increasing cycle number.

Another important issue associated with the electrode material is the surface reaction during the cycling process. To understand this, we measured *ex situ* V L-edge, C and O K-edge XAS of the electrodes at different states of charge through the electrolyte side by both TEY (Figure 5) and TFY modes (Figure S6). The intensity of V L-edge XAS is dynamically changed as a function of the state of charge. As demonstrated in Figure 5a and Figure S6, the V L-edge XAS signal is gradually quenched during discharge (spectra A-E) and partially recovered during charge (spectra E-H). This observation suggests the formation of a SEI layer on the electrode surface, whose thickness swells during discharge and shrinks during charge. The breathing behavior of the SEI layer is also observed throughout the 2nd and 10th cycles, as verified by the intensity change of the V L-edge XAS feature (Figure 5d and Figure S6d). These results indicate that

the formation of the SEI layer on the surface of VS_2 electrode is a highly dynamic process, in contrast to the conventional wisdom that the SEI layer is stable once it is formed.[31,37,46-50]

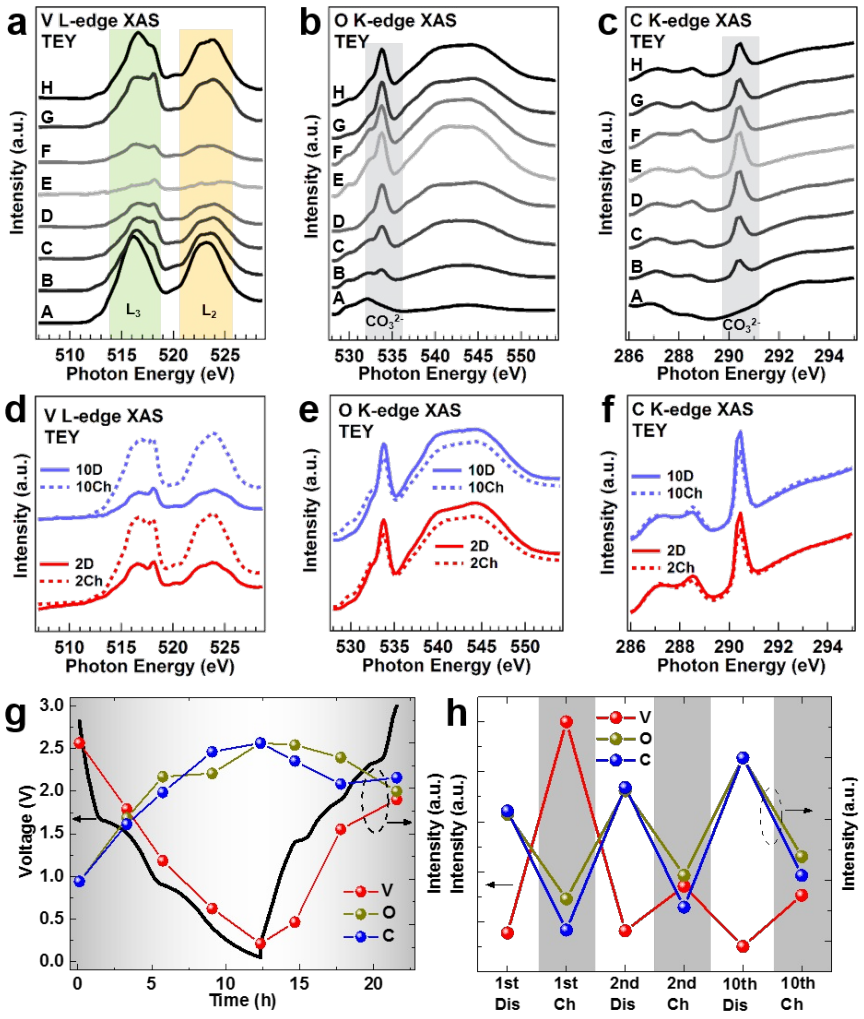

Figure 5. Characterization of the formation process of the SEI layer on the electrode surface. Ex situ V L-edge (a, d), O K-edge (b, e), and C K-edge (c, f) XAS spectra throughout the first, second and tenth cycles, respectively. The XAS spectra were collected on the same samples as the RIXS results through the electrolyte side. Intensity evolution of V L_3-edge feature and carbonate species as a function of discharge/charge states in the first cycle (g) and cycle numbers (h).

The dynamic evolution of the SEI layer is further confirmed by the O K-edge XAS results measured from the same samples, as shown in Figure 5b and Figure S6b. The main feature at 533.8 eV corresponds to the π* peak of carbonate (CO_3^{2-}) groups,[31,46] and its intensity is greatly enhanced during discharge and partially

suppressed during charge. A similar phenomenon is also observed with further cycling (Figure 5e and Figure S6e), suggesting the repeated development and decomposition of carbonate species during the electrochemical processes over extended cycles. The same evolution of the carbonate species is also observed in the C K-edge XAS results (Figure 5c, f and Figure S7c, f). The formation of carbonate species is most likely due to the decomposition of the non-aqueous electrolyte (EC and DEC in our case) at the electrode surface, which is the main component of the formed SEI layer.[37,46] In addition, the intensity variation of the carbonate species is similar for the TEY and TFY spectra (Figure 5 versus Figure S7), strongly indicating that the chemical composition changes throughout the SEI layer during the discharge and charge processes.

To quantitatively understand the development of the SEI layer, we plotted the intensity evolution of the V L_3-edge feature and the carbonate species as a function of states of charge (Figure 5g) and cycle number (Figure 5h). Because the absolute intensity of the TFY signal contains a self-absorption effect, we only use the TEY spectra for this quantitative analysis. It can be clearly seen that the carbonate species are gradually formed during discharge and decomposed during charge, corresponding the increase and decrease of the thickness of the SEI layer, respectively. As a consequence, the intensity of the V L_3-edge feature demonstrates an opposite trend to that of the carbonate species. In addition, it is notable that only apportion of the carbonate species is degraded during charge, resulting in a steady increase of the overall amount of the carbonate species with cycling. This indicates that the formation of the SEI layer on the electrode surface is a dynamic process and the SEI layer with a large amount of carbonate species gradually becomes more extensive over extended cycles. Actually, the dynamic behavior of the SEI layer was also observed for other conversion electrodes in LIBs, e.g., NiO,[37] $ZnFe_2O_4$,[51] and TiS_2,[52] which may suggest that this is a universal behavior for the SEI formation process of conversion-based electrodes.

Conclusions

We have prepared layer-by-layer stacked VS_2 nanosheets via a facile one-step PVP assisted method and then systematically investigated the electrochemical reaction mechanism and formation process of the SEI layer of the VS_2 nanosheets used as the electrode material for LIBs using multimodal *in situ* and *ex situ* X-ray spectroscopies. The VS_2 electrodes experience lithium intercalation and conversion reactions

consecutively during the discharge process and the structure is partially recovered during the subsequent charge process. Both V and S are involved in the redox process during cycling. In addition, we reveal that the electrochemical processes can influence both the oxidation states of V and the hybridization strength between V and S, as directly evidenced by the intensity change of the V-S hybridized states and pure V states as well as the d-d excitations as a function of the state of charge shown in the RIXS results. Furthermore, we provide unambiguous evidence that the formation of the SEI layer on the VS_2 electrode surface is a highly dynamic process: the carbonate species in the SEI layer is developed and partially decomposed during discharge and charge, respectively, with a gradual increase of the overall amount of the carbonate species with cycling. This dynamic formation process of the SEI layer may be a universal phenomenon for conversion-based electrodes. The present study delivers deeper insights into the electrochemical reaction mechanism of TMD based electrodes for LIBs and sheds light on the formation process of the SEI layer, which could be useful for guiding the rational design of other TMD electrode materials to achieve high power and long cycling LIBs.

Supporting information

The supporting information is available free of charge via the Internet at http://pubs.acs.org.

Acknowledgements

The work at the Advanced Light Source of the Lawrence Berkeley National Laboratory was supported by the Director, Office of Science, Office of Basic Energy Sciences, of the U.S. Department of Energy under Contract No. DE-AC02-05CH11231.

References

1. Goodenough, J. B.; Park, K. S. *J Am Chem Soc* **2013,** *135*, 1167.
2. Tarascon, J.-M.; Armand, M. *Nature* **2001,** *414*, 359.
3. Yu, S. H.; Feng, X.; Zhang, N.; Seok, J.; Abruna, H. D. *Acc Chem Res* **2018**.
4. Whittingham, M. S. *Chem Rev* **2014,** *114*, 11414.
5. Mai, L.; Tian, X.; Xu, X.; Chang, L.; Xu, L. *Chem Rev* **2014,** *114*, 11828.
6. Zhou, L.; Zhang, K.; Hu, Z.; Tao, Z.; Mai, L.; Kang, Y.-M.; Chou, S.-L.; Chen, J. *Advanced Energy Materials* **2017**, 1701415.
7. Bruce, P. G.; Freunberger, S. A.; Hardwick, L. J.; Tarascon, J. M. *Nat Mater* **2012,** *11*, 19.
8. Tan, C.; Cao, X.; Wu, X. J.; He, Q.; Yang, J.; Zhang, X.; Chen, J.; Zhao, W.; Han, S.; Nam, G. H.; Sindoro, M.; Zhang, H. *Chem Rev* **2017,** *117*, 6225.

9. Choi, W.; Choudhary, N.; Han, G. H.; Park, J.; Akinwande, D.; Lee, Y. H. *Materials Today* **2017,** *20*, 116.
10. Wang, T.; Chen, S.; Pang, H.; Xue, H.; Yu, Y. *Adv Sci (Weinh)* **2017,** *4*, 1600289.
11. Stephenson, T.; Li, Z.; Olsen, B.; Mitlin, D. *Energy Environ. Sci.* **2014,** *7*, 209.
12. Teng, Y.; Zhao, H.; Zhang, Z.; Li, Z.; Xia, Q.; Zhang, Y.; Zhao, L.; Du, X.; Du, Z.; Lv, P.; Swierczek, K. *ACS Nano* **2016,** *10*, 8526.
13. Jing, Y.; Zhou, Z.; Cabrera, C. R.; Chen, Z. *The Journal of Physical Chemistry C* **2013,** *117*, 25409.
14. Wang, D.; Liu, Y.; Meng, X.; Wei, Y.; Zhao, Y.; Pang, Q.; Chen, G. *J. Mater. Chem. A* **2017,** *5*, 21370.
15. Wang, W.; Sun, Z.; Zhang, W.; Fan, Q.; Sun, Q.; Cui, X.; Xiang, B. *RSC Adv.* **2016,** *6*, 54874.
16. Fang, W.; Zhao, H.; Xie, Y.; Fang, J.; Xu, J.; Chen, Z. *ACS Appl Mater Interfaces* **2015,** *7*, 13044.
17. Zhou, J.; Wang, L.; Yang, M.; Wu, J.; Chen, F.; Huang, W.; Han, N.; Ye, H.; Zhao, F.; Li, Y.; Li, Y. *Adv Mater* **2017**.
18. Sun, R.; Wei, Q.; Sheng, J.; Shi, C.; An, Q.; Liu, S.; Mai, L. *Nano Energy* **2017,** *35*, 396.
19. Yu, D.; Pang, Q.; Gao, Y.; Wei, Y.; Wang, C.; Chen, G.; Du, F. *Energy Storage Materials* **2018,** *11*, 1.
20. Li, W.; Huang, J.; Feng, L.; Cao, L.; Feng, Y.; Wang, H.; Li, J.; Yao, C. *J. Mater. Chem. A* **2017,** *5*, 20217.
21. Liu, X.; Yang, W.; Liu, Z. *Adv Mater* **2014,** *26*, 7710.
22. Li, Q.; Qiao, R.; Wray, L. A.; Chen, J.; Zhuo, Z.; Chen, Y.; Yan, S.; Pan, F.; Hussain, Z.; Yang, W. *Journal of Physics D: Applied Physics* **2016,** *49*, 413003.
23. Zhang, L.; Sun, D.; Feng, J.; Cairns, E. J.; Guo, J. *Nano Lett* **2017,** *17*, 5084.
24. Zhang, L.; Sun, D.; Kang, J.; Feng, J.; Bechtel, H. A.; Wang, L. W.; Cairns, E. J.; Guo, J. *Nano Lett* **2018,** *18*, 1466.
25. Wang, H.; Yi, H.; Chen, X.; Wang, X. *J. Mater. Chem. A* **2014,** *2*, 1165.
26. Mikhaleva, N. S.; Visotin, M. A.; Kuzubov, A. A.; Popov, Z. I. *The Journal of Physical Chemistry C* **2017,** *121*, 24179.
27. Wu, Z.; Ouvrard, G.; Lemaux, S.; Moreau, P.; Gressier, P.; Lemoigno, F.; Rouxel, J. *Physical review letters* **1996,** *77*, 2101.
28. Gorlin, Y.; Patel, M. U. M.; Freiberg, A.; He, Q.; Piana, M.; Tromp, M.; Gasteiger, H. A. *Journal of The Electrochemical Society* **2016,** *163*, A930.
29. Chen, J. L.; Chang, C. C.; Ho, Y. K.; Chen, C. L.; Hsu, C. C.; Jang, W. L.; Wei, D. H.; Dong, C. L.; Pao, C. W.; Lee, J. F.; Chen, J. M.; Guo, J.; Wu, M. K. *Phys Chem Chem Phys* **2015,** *17*, 3482.
30. Wong, J.; Lytle, F. W.; Messmer, R. P.; Maylotte, D. H. *Physical Review B* **1984,** *30*, 5596.
31. Bak, S.-M.; Qiao, R.; Yang, W.; Lee, S.; Yu, X.; Anasori, B.; Lee, H.; Gogotsi, Y.; Yang, X.-Q. *Advanced Energy Materials* **2017**, 1700959.
32. Yoon, J.; Muhammad, S.; Jang, D.; Sivakumar, N.; Kim, J.; Jang, W.-H.; Lee, Y.-S.; Park, Y.-U.; Kang, K.; Yoon, W.-S. *Journal of Alloys and Compounds* **2013,** *569*, 76.
33. Zhou, D.; Permien, S.; Rana, J.; Krengel, M.; Sun, F.; Schumacher, G.; Bensch, W.; Banhart, J. *Journal of Power Sources* **2017,** *342*, 56.
34. Sakuda, A.; Ohara, K.; Fukuda, K.; Nakanishi, K.; Kawaguchi, T.; Arai, H.; Uchimoto, Y.; Ohta, T.; Matsubara, E.; Ogumi, Z.; Okumura, T.; Kobayashi, H.; Kageyama, H.; Shikano, M.; Sakaebe, H.; Takeuchi, T. *J Am Chem Soc* **2017**.
35. Kostov, S.; Strauss, E.; Golodnitsky, D.; Greenbaum, S.; Peled, E. *Journal of power sources* **1999,** *81*, 709.

36. Tao, S.; Huang, W.; Xie, H.; Zhang, J.; Wang, Z.; Chu, W.; Qian, B.; Song, L. *RSC Advances* **2017,** *7*, 39427.
37. Lin, F.; Nordlund, D.; Weng, T. C.; Zhu, Y.; Ban, C.; Richards, R. M.; Xin, H. L. *Nat Commun* **2014,** *5*, 3358.
38. Poizot, P.; Laruelle, S.; Grugeon, S.; Dupont, L.; Tarascon, J. *Nature* **2000,** *407*, 496.
39. Yang, W.; Liu, X.; Qiao, R.; Olalde-Velasco, P.; Spear, J. D.; Roseguo, L.; Pepper, J. X.; Chuang, Y.-d.; Denlinger, J. D.; Hussain, Z. *Journal of Electron Spectroscopy and Related Phenomena* **2013,** *190*, 64.
40. Horrocks, G. A.; Braham, E. J.; Liang, Y.; De Jesus, L. R.; Jude, J.; Velázquez, J. M.; Prendergast, D.; Banerjee, S. *The Journal of Physical Chemistry C* **2016,** *120*, 23922.
41. Maganas, D.; Roemelt, M.; Havecker, M.; Trunschke, A.; Knop-Gericke, A.; Schlogl, R.; Neese, F. *Phys Chem Chem Phys* **2013,** *15*, 7260.
42. Schmitt, T.; Duda, L. C.; Matsubara, M.; Mattesini, M.; Klemm, M.; Augustsson, A.; Guo, J. H.; Uozumi, T.; Horn, S.; Ahuja, R.; Kotani, A.; Nordgren, J. *Physical Review B* **2004,** *69*.
43. Khyzhun, O. Y.; Strunskus, T.; Grünert, W.; Wöll, C. *Journal of Electron Spectroscopy and Related Phenomena* **2005,** *149*, 45.
44. Groot, F. d.; Kotani, A., *Core Level Spectroscopy of Solids*. CRC Press: 2008.
45. Abe, H.; Terauchi, M.; Tanaka, M.; Shin, S.; Ueda, Y. *Japanese journal of applied physics* **1997,** *36*, 165.
46. Zhuo, Z.; Lu, P.; Delacourt, C.; Qiao, R.; Xu, K.; Pan, F.; Harris, S. J.; Yang, W. *Chem Commun (Camb)* **2018**.
47. Owejan, J. E.; Owejan, J. P.; DeCaluwe, S. C.; Dura, J. A. *Chemistry of Materials* **2012,** *24*, 2133.
48. Peled, E.; Menkin, S. *Journal of The Electrochemical Society* **2017,** *164*, A1703.
49. Gauthier, M.; Carney, T. J.; Grimaud, A.; Giordano, L.; Pour, N.; Chang, H. H.; Fenning, D. P.; Lux, S. F.; Paschos, O.; Bauer, C.; Maglia, F.; Lupart, S.; Lamp, P.; Shao-Horn, Y. *J Phys Chem Lett* **2015,** *6*, 4653.
50. Yu, X.; Manthiram, A. *Energy & Environmental Science* **2018**.
51. Rezvani, S. J.; Nobili, F.; Gunnella, R.; Ali, M.; Tossici, R.; Passerini, S.; Di Cicco, A. *The Journal of Physical Chemistry C* **2017,** *121*, 26379.
52. Zhang, L. *Unpublished Results* **2018**.